Design and Validation of a New PPG Module to Acquire High-Quality Physiological Signals for High-Accuracy Biomedical Sensing

Yung-Hua Kao, Paul C.-P. Chao, *Senior Member, IEEE*, and Chin-Long Wey, *Life Fellow, IEEE*

***Abstract*—A new photoplethysmography (PPG) module is designed, optimized, and fabricated in this study to obtain quality PPG signal for high-accuracy bio-sensing. The module contains four light emitting diodes (LEDs) in wavelengths of 530, 660, 850, and 940 nm and a photo-diode (PD). The distances between LEDs and PD are optimized for quality PPG signals via maximizing the ratios of pulsatile (ac) to non-pulsatile (dc) components in PPG waveforms. The optimization is carried out based on an establishment of a complete optical model that simulates well optics under the user's skin based on Beer–Lambert law. In results, the optimal LED/PD distances that lead to maximal ac/dc ratios of PPGs for different wavelengths are derived. With the optimal LEDs/PD distances in hand, a new PPG module is designed and fabricated subsequently, and further installed in a hand-held blood pressure (BP) sensing device for performance validation. Based on experimental results, for the PPG module, an ac/dc ratio of 8.02% is achieved by the proposed PPG module as opposed to 6.74% and 6.90% by two other commercial modules. As for sensing BP based on reflective pules transient time, the error is controlled well with the mean difference (MD) and standard deviation (SD) as -1.16 ± 5.38 (MD$\pm$SD) and -0.53 ± 1.92 mmHg, respectively, for systolic blood pressure and diastolic blood pressure. The resulted accuracy successfully categories the developed PPG sensor among the bests by Association for the Advancement of Medical Instrumentation and British Hypertension Society.**

***Index Terms*—Photoplethysmography (PPG) Sensor, LED/PD PPG module, blood pressure (BP) measurement, reflective pules transient time (R-PTT).**

Manuscript received April 4, 2018; revised July 15, 2018; accepted September 11, 2018. Date of publication September 24, 2018; date of current version October 19, 2018. This work was supported by in part by the Ministry of Science and Technology (MOST), Taiwan under Grant MOST107-3017-F009-003; in part by the Center for Emergent Functional Matter Science of National Chiao Tung University and the Center For Intelligent Drug Systems and Smart Bio-devices (IDS2B) from The Featured Areas Research Center Program within the framework of the Higher Education Sprout Project by the Ministry of Education (MOE) in Taiwan; in part by the Novel Bioengineering and Technological Approaches to Solve Two Major Health Problems in Taiwan sponsored by the Taiwan MOST Academic Excellence Program under Grants MOST 106-2633-B-009-001 and 107-2633-B-009-003; in part by Epistar Corporation; in part by Chunghwa Picture Tubes, Ltd.; and in part by MOST under Grants 106-2221-E-009-089, 106-2218-E-009-011, 106-2634-F-009-001, 106-2119-M-492-001, 107-2221-E-009-166, 107-2118-E-009-006, and 107-2218-E-009-006. *(Corresponding author: Paul C.-P. Chao.)*

The authors are with the Department of Electrical Engineering, National Chiao Tung University, Hsinchu 300, Taiwan (e-mail: yunghwa.kao@gmail.com; pchao@mail.nctu.edu.tw; clwey@nctu.edu.tw).

Color versions of one or more of the figures in this paper are available online at http://ieeexplore.ieee.org.

Digital Object Identifier 10.1109/JSTQE.2018.2871604

I. Introduction

MUCH recent research effort has been dedicated to the development of a portable and/or wearable photoplethysmography (PPG) bio-sensors for various physiological measurements [1]. Most of PPG sensors are designed for measuring non-invasively the blood volume pulses (BVPs) or blood flow (BF) in the vascular/microvascular bed underneath the skin tissue [2]. One of much noted applications is for measuring cuffless blood pressure (BP). Many studies have assured strong relevance between high BP and CVD [3]. According to the reported study [4], a decrease in systolic blood pressure (SBP) by 10 mm-Hg would reduce chance of CVD by 20%, coronary heart disease by 17%, stroke by 27%, and heart failure by 28%. Therefore, prevention, treatment, and control of elevated BP is always an important task for CVD prognosis.

In general, a conventional blood pressure (BP) monitor adopts a pumping cuff to apply pressure on users. This cuff is usually of large sizes and heavy weights; thus, not easily designed for portability and then unsuitable for long-time usage and data collection. However, in clinical practices, long-time BP data collection is important for giving therapy. To realize continuous, comfortable and long-time monitoring and collecting BP data, many cuff-less and noninvasive blood pressure sensors have been proposed recently [5]–[11].

To date, most of cuffless BP sensor under intensive effort of development can be categorized into two different types. They are contact-type vibration sensors and photoplethysmography (PPG) sensors. For the contact vibration sensor, Kaniusas [7] proposed a magnetoelastic vibration sensor of skin curvature to realize continuous BP measurement with assistance of an ECG sensor. Similar to this vibration sensor at wrist arterial are the works reported by Tu *et al.* [8], [9], where a strain-type vibration sensor was proposed. Despite the advantage of cufflessness, the works in [7]–[9] inevitably experience sensing inaccuracy due to mis-positioning of the vibration sensor on the small wrist arterial spot where there is maximum pulsation. As for the optical PPG sensor, it can easily work against moderate mis-positioning. However, the optical PPG sensors instead suffer seriously from a very small pulsatile (AC) component embedded in a highly-noisy and drifting non-pulsatile (DC) component in a practical measured PPG waveform, leading to inaccurate bio-sensing based on the small and noisy AC component [11].

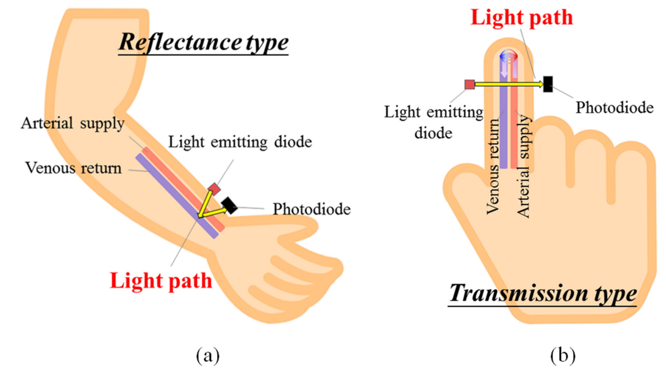

Fig. 1. Two different modes of PPG sensing. (a) The reflectance mode. (b) The transmission mode.

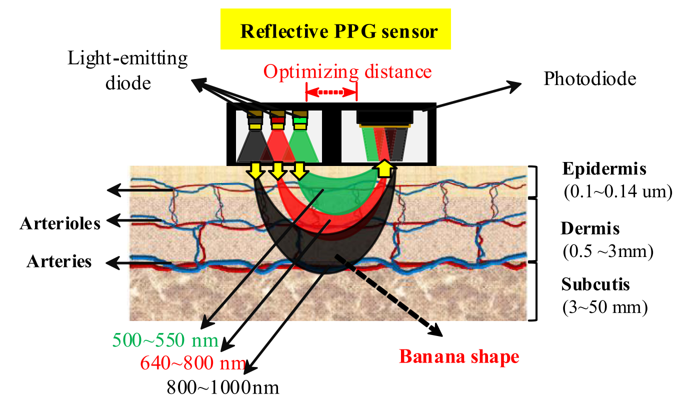

Fig. 2. Illustration of skin vascular bed with reflectance PPG sensor.

To remedy the problem, this study is dedicated to design and fabricate a new PPG module with its AC maximized via optimizing the distances between LEDs and PD in the designed PPG module for maximal ratios of pulsatile (AC) to non-pulsatile (DC) components in measured PPG waveforms. This maximization on the AC/DC ratios is carried out based on an establishment of a complete optical model that simulates well optics under the user's skin based on Beer-Lambert law [12]–[17]. The obtained optimal LEDs/PD distances that lead to large AC/DC ratios are implemented in a fabricated PPG module and further installed in a hand-held blood pressure (BP) sensing device for performance validation.

This paper is organized as follows. Section II introduces the technology and principles of the photoplethysmography (PPG) sensor. Section III unveils the design and simulation of the proposed PPG module in details. Section IV elaborates the blood pressure (BP) sensing using the designed PPG module. Section V presents measurement results, followed by conclusions in Section VI.

II. Photoplethysmography (PPG) Sensor

A. PPG Technology

The technology of photoplethysmography (PPG) sensing has been widely employed for detecting non-invasive of human tissues [18]. The PPG sensor owns the merits of non-invasiveness, simple and small form factor and low-cost. Only a few electro-optic components are needed to implement PPG. A typical PPG module consists of light source, e.g., light emitting diodes (LEDs) illuminating the tissue and a photo-diode (PD) receiving the small fluctuations in the received light intensity due to pulsating blood vessels in size. And the pulsation of vessels are caused by fluctuating pumping power from subject's heart. Thus, the main frequency of the PPG waveform synchronizes with subject's heartbeat.

There are two different measuring modes of PPG sensing. One is the reflectance mode while another is transmission mode, as illustrated in Fig. 1(a) and (b). For the reflectance mode, LEDs and PD are at the same side, while at different sides for the transmission mode. The transmission-mode PPG sensors are usually placed near finger tips for minimum required transmitted intensity, while the reflectance-mode sensors can be placed at the spots where blood vessels are close to skin surface. In this study, effort is dedicated particularly to the reflectance-mode PPG for acquiring high-quality PPG waveform from pulsating radial arteries at subject's wrist, as illustrated in Fig. 1(a). The signal quality level achieved by radial arteries is substantially higher than at fingertip by the transmission mode, since the sizes of blood vessels at fingertips are much smaller than radial arteries at the wrist.

B. Working Principles

For the reflectance-mode PPG sensors, the optical power transmission from LED to PD, as shown in Fig. 2, experiences highly scattering substances, such as epidermis, dermis, subcutaneous tissues and pulsating capillaries, arterioles and arteries. Based on Beer-Lambert law, the optical path of most of the optical power received by PD follows generally banana shapes as shown in Fig. 2 [19], for the reflectance PPG sensor. Longer wavelength leads to larger size of the banana [13]–[17]; in other words, penetrating deeper under skin. In fact, the optical power emitted by the LED attenuates along the optical banana-shape path due to the scattering and absorption through all tissues, blood and vessel walls, which can be characterized by the changes in the coefficient of absorption, i.e.,

$$A_{p\lambda} = -\log \frac{L_{Tp\lambda}}{L_{Ip\lambda}} = \mu_{a\lambda} \cdot l_{p\lambda} \tag{1}$$

where the subscript p refers to the power of a given light trace in the banana shape; λ denotes the wavelength of the light trace; $\mu_{a\lambda}$ is the absorption coefficient along a given light trace; $l_{p\lambda}$ is the emission power from an LED for a given light trace; $L_{Tp\lambda}$ is the light intensity of a transmitted light in the light trace in the banana shape; $L_{Ip\lambda}$ the light intensity of the incident light along the banana; $A_{p\lambda}$ is the resulted overall absorbance along a given light trace from LED to PD. Note that Eq. (1) is similar to the common phenomenological analysis as described in many works such as [20]–[22].

C. Characteristics of PPG

Along the optical path of optical power attenuation in Fig. 2 following banana-shape traces, all the factors leading to

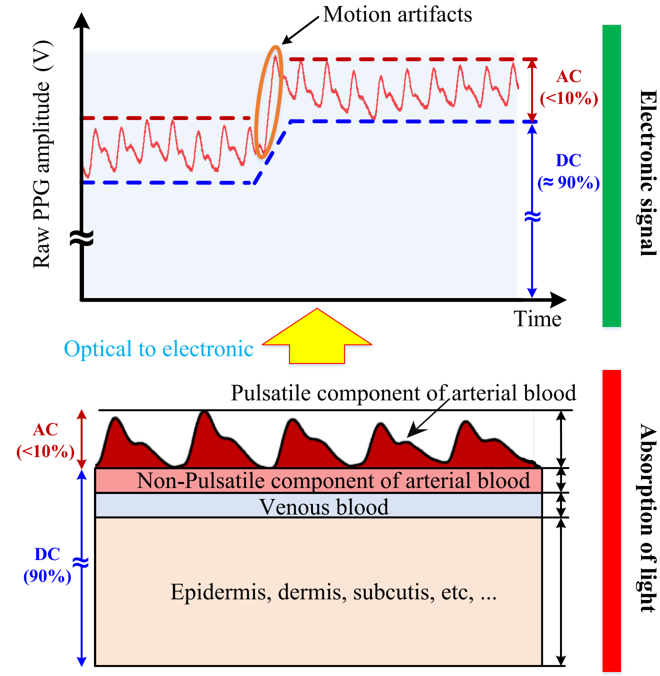

Fig. 3. Principles of conversion of light intensity into electronic signal.

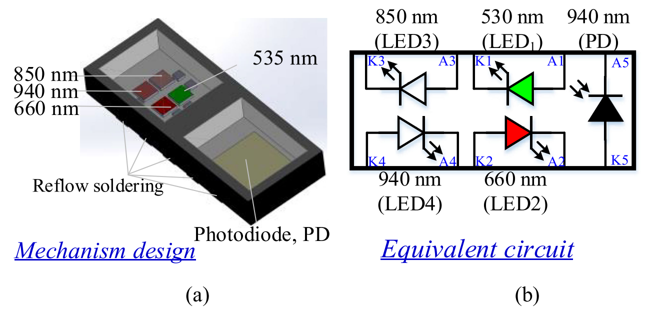

Fig. 4. The fabricated bio-sensor module. (a) The mechanism design. (b) Equivalent circuit.

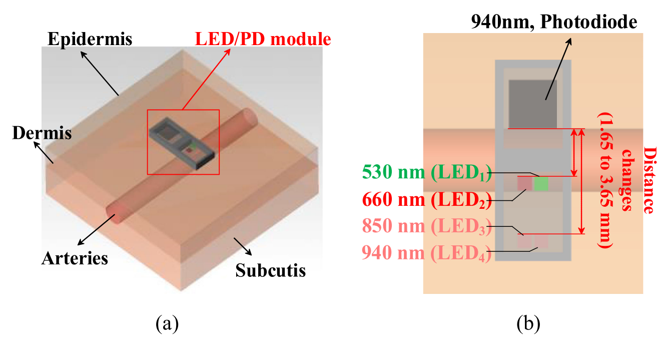

Fig. 5. Bio-optical modeling. (a) The simulation model by optical software. (b) Top view over the bio-sensor module in the bio-optical model.

attenuation are theoretically stationary except for those due to absorption by chromophores in pulsating capillaries, arterioles and arteries, which leads to fluctuating power received by PD. Therefore, a typical measured PPG waveform consists of two components, non-pulsatile and pulsatile ones, as illustrated by Fig. 3. The non-pulsatile component (e.g., DC) is the average power received by the PD due to light diffraction, reflectance and absorption under skin through epidermis, dermis, sub-cutis, venous blood and non-pulsatile part of arterial blood along the banana path based on the aforementioned Beer-lambert law Eq. (1) as illustrated in Fig. 2, while the pulsatile component (e.g., AC) is due to the fluctuation in the optical absorption by chromophores in pulsating blood vessels, like capillary, arterioles and arteries. Since along the topical path the optical power received by PD experiences very small area of blood vessels, and, furthermore, if the distance between LED and PD does not match the size of the banana for a given wavelength, the pulsating AC component is about only 1–10% of the measured PPG waveform or even smaller, while the non-pulsating AC one is as large as 90–99% [23].

Thus, the pulsating component of raw PPG waveforms from PD is usually too noisy to be processed directly for bio-sensing such as for heartbeat, blood pressure, blood flow and/or blood sugar. Moreover, the non-pulsatile component is not even stationary due to environmental lighting interference, motion artifacts from moving subjects and noises from all opto-electronic devices employed in the PPG sensor, as also shown in Fig. 3. Although one can usually design some post signal processing techniques to overcome the aforementioned difficulties, the distortion on the original PPG signals is unavoidable. To maximize the bio-sensing accuracy, this study designs a new PPG module with aim to find the optical distance between LED and PD for a given wavelength. In this way, the pulsatile (AC) component can be maximized as opposed to its non-pulsatile (DC) counterpart to result in high-quality pulsatile PPG components prior to application of digital signal processing for biological sensing.

III. Design of a New PPG Module

A. *The New Module*

A new reflective PPG module as shown in Fig. 4(a) is designed and realized by this study to demonstrate the effectiveness of the proposed method to maximize the pulsatile component as opposed to non-pulsatile counterpart in PPG waveform. This new module consists of two compartments. One accommodates four LEDs emitting light with different wavelengths, 530, 660, 850 and 940 nm, while another contains a single PD with a wide wavelength absorption range. The size of the module is minimized to 7 mm × 2.7 mm × 1.2 mm, a small form factor that makes it easy to be integrated into portable or wearable devices in applications [24]. A separating black wall is between the two compartments, which is designed to prevent direct interference from LEDs to PD. Reflow soldering is applied for mounting four LEDs and the PD onto a small-sized PCB attached to the bottom surface of the designed new module. Fig. 4(b) depicts the equivalent circuit of this designed PPG module.

B. *Optical Simulation Model*

An optical simulation model as depicted in Fig. 5(a), is established, which consists of the proposed LEDs/PD module, epidermis, dermis, sub-cutis, capillaries, arterioles and radial artery. The associated optical properties used for simulation are

TABLE I
BIO-OPTICAL PROPERTIES OF HUMAN TISSUES WITH REFLECTIVITY AND SCATTERING MEDIUM

No.	Materials	Parameters				
		Thickness	*Refractive Index*	*Absorption* [/mm]	*Scattering anisotropy*	*Scattering coefficient* (1/mm)
1	Epidermis	0.14 mm	1.40	0.50 @ 530 nm 0.26 @ 660 nm 0.12 @ 850 nm 0.06 @ 940 nm	0.8	31.3 @ 530 nm 22.1 @ 660 nm 17.4 @ 850 nm 16.0 @ 940 nm
2	Dermis	2.6 mm	1.50	0.28 @ 530 nm 0.15 @ 660 nm 0.10 @ 850 nm 0.08 @ 940 nm	0.8	19.2 @ 530 nm 14.4 @ 660 nm 10.5 @ 850 nm 9.70 @ 940 nm
3	Subcutis	4 mm	1.44	0.28 @ 530 nm 0.40 @ 660 nm 0.13 @ 850 nm 0.08 @ 940 nm	0.8	16.3 @ 530 nm 12.3 @ 660 nm 9.60 @ 850 nm 8.90 @ 940 nm
4	Arteries	2 mm (DC) 2.2 mm (AC)	1.40	180 @ 530 nm 1.88 @ 660 nm 4.65 @ 850 nm 5.87 @ 940 nm	0.95 @ 530 nm 0.98 @ 660 nm 0.98 @ 850 nm 0.97 @ 940 nm	701 @ 530 nm 894 @ 660 nm 804 @ 850 nm 710 @ 940 nm
5	Air	-	1.00	-	-	-

listed in Table I, where the thicknesses, coefficients of thickness, refraction, absorption, scattering and scattering anisotropy are given for accurate simulation. The thicknesses of different layers assumed in this study herein are in accordance with those presented as 0.1 to 0.14 mm for epidermis, 0.5 to 3 mm for dermis, and 3 to 50 mm for sub-cutis. The wrist artery is assumed pulsating between the 2 and 2.2 mm [19]. Thus, the light intensity reaching the PD includes two components by simulations, a non-pulsatile component as a DC, while another pulsatile pulsation as an AC component. Finally, the total ray number of light trace is raised to as high as 20 million to achieve solid conclusion for optical design in the next section.

C. Determining Distances Between LEDs/PD

With the simulation model of the LEDs/PD module as shown in Fig. 5(a, b) built, the distances between LEDs and PD in the module are determined to render the best signal quality for satisfactory estimations on bio-signs, such as heart beat, blood pressure and blood flow. To this end, the pulsatile (AC) component in the measured PPG waveform is to be maximized as opposed to its non-pulsatile (DC) counterpart, with aim to result in favorable signal-to-noise ratios (SNRs) of the AC component for estimating various bio-signs with satisfactory accuracy. The optimization goal is thus set up as to maximize the ratio of AC/DC for pairs of the LED at a given wavelength and the PD.

The optimization is proceeded with considering a number of LED/PD distances between 1.65 to 3.65 mm with an increment of 0.1 mm for simulations via TracePro. The results are shown in Fig. 6, where the AC/DC ratios versus the varying LED/PD distance for four pairs of LED/PD in different wavelengths are depicted. It is seen from this figure that each wavelength renders its optimum at some LED/PD distance. Maximum AC/DC ratios occur at the LED/PD distances of 1.85, 2.35, 2.75 and 2.75 mm, respectively, for wavelengths of 530, 660, 850, 940 nm. The associated lighting traces simulated are shown in Fig. 7(a–d),

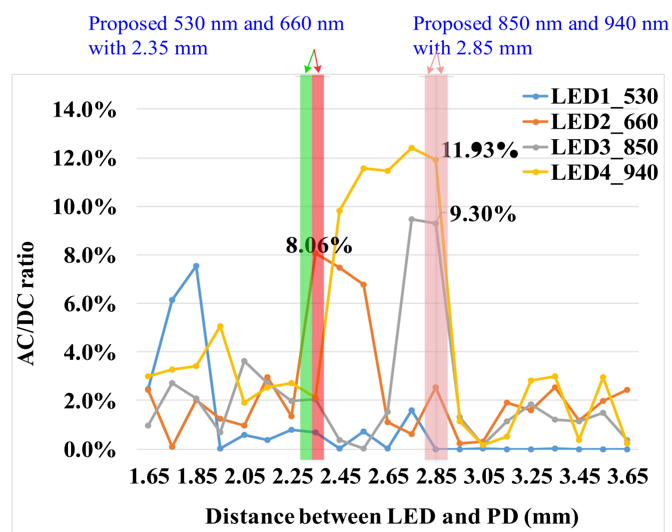

Fig. 6. The power received by PD with varied distance to LED and wavelength, in term of AC-to-DC ratio for maximizing S/N ratio.

where banana effects based on Beer-Lambert Law are clearly seen.

It appears in Fig. 6 that larger wavelengths of 850 and 940 nm lead to better pulsatile component received by PD at longer distances than shorter 530, 660 nm. This is due to the fact that the LED lighting in 850 and 940 nm as infrareds penetrate deeper than 530, 660 nm to reach radial arteries in the subcutis, where the radial arteries are in much larger sizes than capillaries and arterioles, thus resulting in larger pulsatile AC components in PPG. These deeper penetrations are also evidenced from Fig. 7, where the light traces of 850 and 940 shape larger banana shapes and reach arteries in the subcutis, while 530, 660 nm do not. As for 530 (green) and 660 (yellow) nm, their maxima in Fig. 6 occur at the LED/PD distances at closer 1.85 and 2.25 mm, as their emission penetrates shallower into the depths where there

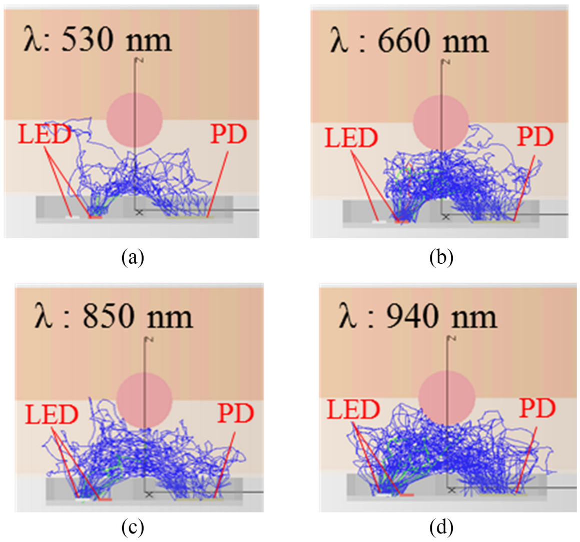

Fig. 7. Side view of banana effect producing multiple scattered light traces. (a) 530 nm. (b) 660 nm. (c) 850nm. (d) 940 nm.

are capillaries layer in epidermis and arterioles layer in dermis, respectively [25]. This is also evidenced in Fig. 7 where the bananases of 530, 660 nm penetrate less deeper than 850 and 940 mm. In short, while aiming for accurate bio-sensing based on PPG, the best choice is to adopt 940-nm LED for maximum AC/DC ratios of measured PPG as shown in Fig. 6. This finding is consistent to a number of published medical works, such as [26], [27].

IV. Sensing Blood Pressures

The designed LED/PD module is next adopted for blood pressure (BP) sensing to validate its favorable performance against other commercial modules. To this end, the readout circuitry is first designed and implemented for processing output current of the PD, which is followed by developing an algorithm to estimate BPs [28].

A. Readout Circuitry

A readout circuitry is designed and realized to convert the output current of the PD in the designed PPG module to digital values of PPG for estimating BPs. The architecture of the entire readout circuitry is schematically shown in Fig. 8 in blocks. The circuitry includes the equivalent circuits of the reflective PPG sensor, hardware and software. The hardware is implemented on a print circuit board (PCB) and further accommodated into a hand-held BP monitoring device as shown in Fig. 9, while the software is implemented in a laptop. The data transmission from the hand-held device to the laptop is completed via Bluetooth. Designed and installed in the laptop is a graphical user interface (GUI) to monitor in real time the measured PPG waveform and estimated BPs.

The sub-circuits on the PCB for hardware include an analog front-end (AFE) of a trans-impedance amplifier (TIA), a programmable gain amplifier, a filter, an analog-to-digital converter (ADC), a micro control unit (MCU), a register array, a digital-to-analog converter (DAC), a LED driver and a wireless module as shown in hardware system of Fig. 9. The TIA consists of a differential current-to-voltage (I-V) amplifier that converts the PD current into an appropriate voltage. The measured PD current in raw PPG signals is approximately from 0.5 to 35 μA. The feedback resistor (R_f) of the TIA is programmable between 10 kΩ to 11 MΩ, to be applicable to a wide range of PD current. The feedback capacitor (C_f) is also programmable from 5 to 250 pF. After TIA is a programmable gain amplifier offering gains of 0 dB, 3.5 dB, 6 dB, 9.5 dB, and 12 dB, in order to tune the PPG signal to near full dynamic range before entering a 22-bit ADC. Between ADC and gain amplifier is a band-pass filter to remove the slow-drifting DC caused by motion artifacts and breathing, and high-frequency noises due to environmental lighting and electronics. The acquired digital PPG signals after the ADC are fed back to a register to customize the cut-off frequencies of the band-pass filter and emitting power of LEDs for the user with different skin color. The emitting power of LEDs are tuned by the DAC and a driver circuit. The DAC is of 8-bit resolution to tune the current to drive LEDs within a range from 0 to 200 mA.

As for the software of the readout circuitry as shown in Fig. 8, it consists of a digital filter, baseline correction, period and dynamic range check, heartbeat detection, reflected wave detection, feature extraction for reflective pulse transient time (R-PTT) and calculation for BP.

B. Blood Pressure Algorithm

With quality PPG waveform obtained, the blood pressures can be calculated based on the theory of pulse wave velocity (PWV). According to Bramwell-Hill equation [29], PWV is a function of the density of blood, ρ, and the volume of blood in artery, V, following

$$PWV = \sqrt{\frac{V}{\rho} \frac{(SBP - DBP)}{\Delta V}}, \tag{2}$$

where SBP refers to systolic blood pressure while DBP does diastolic blood pressure. Due to the fact that the blood density, the blood volume in artery, and the change in blood volume are nearly constant for each subject, Eq. (2) can be expressed in a different form of

$$SBP - DBP = \frac{\rho \Delta V}{V} \left(\frac{L}{PTT} \right)^2 = K_a \cdot \frac{1}{PTT^2}, \tag{3}$$

where PTT is the pulse transit time and K_a is a fixed parameter to be calibrated via experiment for a specific subject. The pulse transient time is defined as a period for the pulse wave of blood flow to propagate for some distance in an arterial vessel. In this study, one of PPTs, the reflective PTT (R-PTT), is considered for estimating blood pressures (BPs) based on theory of pulse wave velocity (PWV). This R-PTT is the duration for the pulse wave to propagate from the radial artery (at the location where there is wrist pulsation) in forward direction to the end of the limb and reflected back to the radial artery as a back-propagating pules wave [30]–[33]. The forward pulse wave pumped from heart is called percussion wave, while the reflected wave is reflected

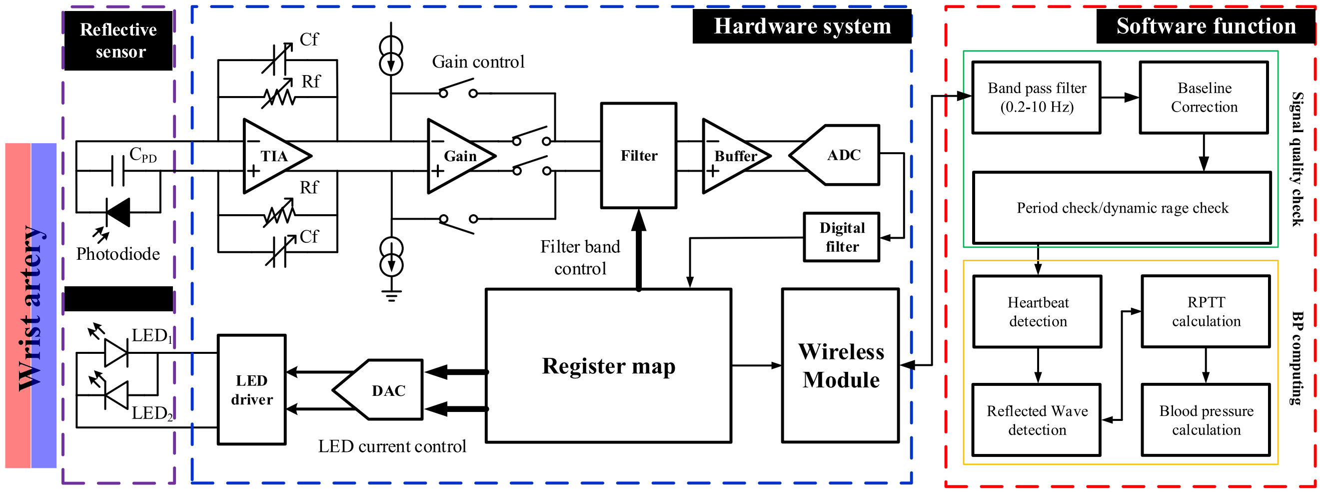

Fig. 8. Functional blocks of the PPG readout circuitry for optical BP measurement.

Fig. 9. The developed hand-held BP monitoring device.

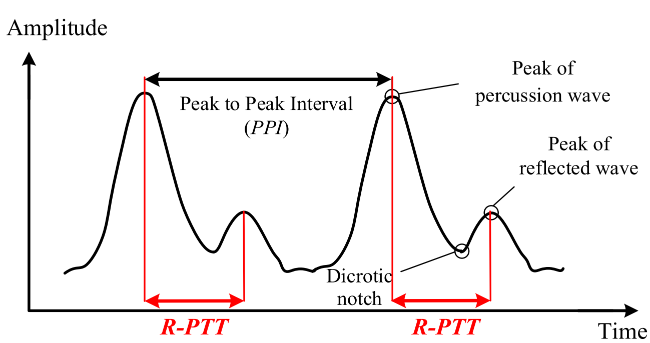

Fig. 10. A typical PPG signal with reflected pulse transit time (R-PTT) featured.

wave. The R-PTT can be captured well by the duration between the 1st and 2nd peaks of a single cardiac PPG waveform, as shown in Fig. 10 [34]. And then BPs can be well estimated by this R-PTT based on the PWV theory. With R-PPT as PPT, based on Eq. (3), SBP can be derived by

$$SBP = DBP + K_a \cdot \frac{1}{R\text{-}PTT^2}. \tag{4}$$

On the other hand, PWV can expressed in terms of the elastic modulus of artery, E_{in}, the thickness of the artery, *h*, the radius of artery, *r*, and the density of blood, ρ, by the Moens-Korteweg equation [35], [36], yielding

$$PWV = \sqrt{\frac{E_{in} h}{2\rho r}}. \tag{5}$$

Based on the experiment results obtained by [37], the elastic modulus of artery is

$$E_{in} = 1428.7e^{0.031 \times MBP}, \tag{6}$$

where MBP is mean blood pressure, which can be re-presented by

$$MBP = K_b + \frac{2}{0.031}\ln\left(\frac{K_c}{R\text{-}PTT}\right), \tag{7}$$

where K_b and K_c are also fixed parameters to be calibrated via experiment for a specific subject. MBP can be estimated by

$$MBP = \frac{1}{3}SBP + \frac{2}{3}DBP. \tag{8}$$

Substitution of Eq. (8) into (4) and (7), DBP can be derived by

$$DBP = K_b + \frac{2}{0.031}\ln\frac{K_c}{R\text{-}PTT} - \frac{1}{3}\frac{K_a}{R\text{-}PTT}. \tag{9}$$

With extracted R-PTTs from measured PPG waveforms by the developed handheld BP sensor and SBPs/DBPs obtained from gold standard BP monitor, one is able to calibrate the parameter of K_a, K_b and K_c based on Eqs. (4) and (9).With determined K_a, K_b and K_c, the developed BP sensor with the LED/PD module inside is ready for sensing SBP and DBP with satisfactory accuracy.

V. Experimental Validation

The LED/PD module proposed in section III-A is fabricated and tested for its signal quality. Moreover, the module is installed in the handheld BP monitor as presented in Fig. 9 to validate its expected performance for BP sensing.

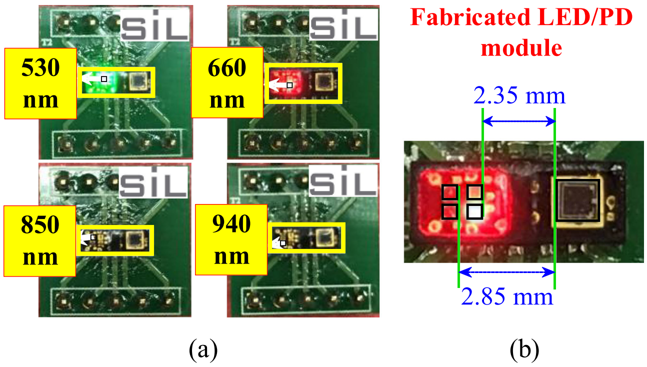

Fig. 11. (a) The fabricated PPG module with different wavelength-LED emitted. (b) LED/PD distances denoted.

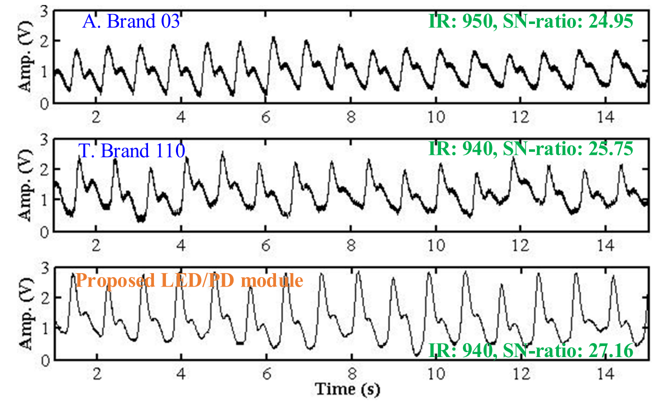

Fig. 12. Measured PPG wave using three different PPG LED/PD modules.

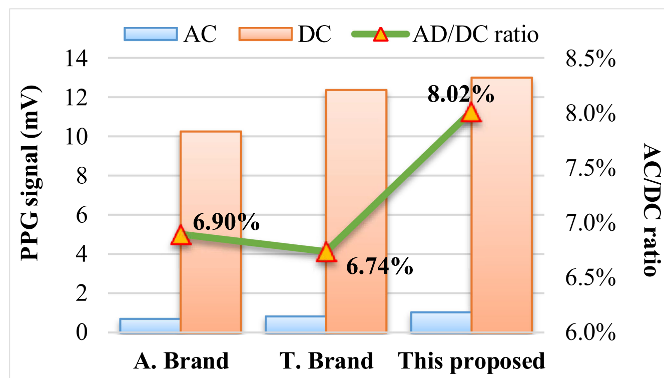

Fig. 13. Measured pulsatile (AC) component, non-pulsatile (DC) component, and their ratios.

A. The PPG Module

The PPG module as pre-designed with four LEDs of different wavelengths in 530, 660, 850 and 940 nm inside is successfully fabricated, as shown in Fig. 11(a–d). Following the simulation and optimization results in Section III, four LEDs in this module are mounted at the bottom PCB at locations conforming to those leading to peaks of AC/DC ratios in Fig. 6. As indicated in Fig. 6, the 850 and 940-nm LEDs are mounted at the location in a distance of 2.85 mm from PD, as seen in Fig. 11(e). This location is very close to those leading to their peaks of AC/DC ratios, 9.3% and 11.93%, respectively, in Fig. 6. Also, the 660-nm LED is mounted at 2.35 mm away from PD to render the maximum peak of AC/DC ratio, also as seen in Fig. 11(e). As for the 530-nm LED, it is not placed at location with the LED-PD distance near 1.85 mm to render the maximum peak of AC/DC ratio. It is instead placed at the same distance of 2.35 mm as 660-nm as also seen in Fig. 11(e) to minimize the overall size of the LED/PD module. The resulted disadvantage of this low AC/DC ratio by 530-nm LED is compensated by increasing emittance of this LED and a higher-order low-pass filter to remove the non-pulsatile DC component in the PPG waveform.

With the new LED/PD module fabricated, effort is next dedicated to measure PPG waveforms at the location of wrist artery for a number of subjects, with aim to validate expected performance. Aside from the proposed module, two other commercial modules available are considered for comparison. One is from Model 03 of Brand A, while another from Model 110 of Brand T. PPG waveforms are measured from the wrist artery of a specific subject using infrared LEDs of three different modules. The wavelengths of Brand A, 03 and Brand T, 110 are 950 and 940 nm, respectively. Raw PPG signals from PDs are processed by a basic second-order low-pass filter to result in the PPG waveforms as shown in Fig. 12. It can be seen from this figure that the proposed LED/PD renders the largest pulsatile (AC) component as compared to the other two commercial modules. The ratios of pulsatile (AC) to non-pulsatile (DC) components are also calculated, as shown in Fig. 13, where it is obviously seen that the proposed module offers the best performance of a LED/PD PPG module in term of the AC/DC ratio, achieving the maximum ratio of 8.02%, as opposed to 6.74% and 6.90% by two other commercial modules. This is due to the in-depth effort dedicated to optimizing the distances between LEDs and PD by this study, as presented in Section III-C. On the other hand, it should be noted at this point that the obtained 8.02% by experiment is slightly lower than its simulated counterpart of 11.93% as presented in Fig. 6. This is due to the signal attenuation effect by the adopted filtering in experiment. Finally, a summary on performance comparison between commercial and proposed modules is given in Table II, where the AC/DC

TABLE II
PERFORMANCE COMPARISON AMONG VARIED PPG MODULES

	A. Brand, 03	A. Brand, 06	T. Brand, 110	**The proposed sensor**
Package size (mm)	9.8×4.3×1.3	9.7×4.2×1.2	7.2×3.6×1.1	**7×2.7×1.2**
LEDs wavelengths (nm)	660/950	590/660/ 810/905	530/665/ 940	**530/660/ 850/940**
Number of LEDs and PDs	LED: 2, PD: 1	LED: 4, PD: 1	LED: 3, PD: 1	**LED: 4, PD: 1**
Optimized distances between LEDs and PD	N/A	N/A	N/A	**Yes**
Achieved AC/DC ratios	6.90 %	N/A	6.74 %	**8.02 %**
Applications	• HR • PPG • SpO2	• HR • PPG • SpO2	• HR • PPG • SpO2	**• HR • PPG • SpO2 • BP • BF**

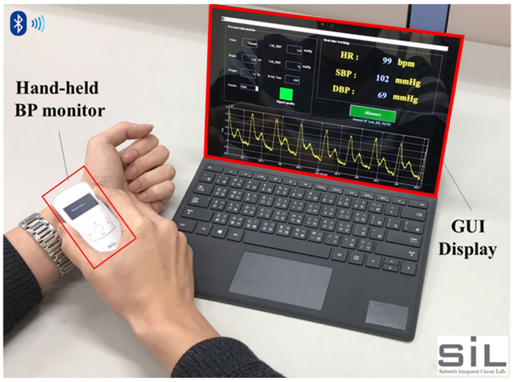

Fig. 14. The setup for experimental BP measurements.

TABLE III
STATISTICS ON SUBJECTS

Parameters	Mean	Range	Number
Male	-		13
Female	-		7
Height (cm)	169	151-180	-
Weight (kg)	62	47-82	-
Age (years)	26	23-36	-
SBP (mmHg)	113	80-151	-
DBP (mmHg)	69	51-95	-
HR (bpm)	78	56-111	-

ratio of 8.02% offered by the proposed module provides the best chance to achieve satisfactory accuracy of bio-sensing using a PPG LED/PD module.

B. BP Sensing

The proposed LED/PD module is incorporated into a BP sensor as shown in Fig. 9. PPG waveforms are measured using the BP sensor for 20 subjects aged between 21 to 34 years old. The setup for measurement is shown in Fig. 14 by a photo. The statistics of other attributes of subjects are listed in Table III. The data is acquired strictly following the international protocol by European society of hypertension (ESH). All subjects are refrained from caffeinated drinks, smoking or eating in the 30 min prior to measurements. Measurements start from a pre-calibration process, which requires to place the BP optical sensor at the spot where one can feel maximum pulsation at wrist above the radial artery, as shown in Fig. 14. A reference commercial blood pressure monitor, OMRON HEM-7310, is used to also measure the blood pressures for calibrating the developed sensor, with K_a, K_b and K_c in Eqs. (4) and (9) calibrated. After calibration, PPG pulsation waveforms are successfully measured. R-PTTs are extracted by the MCU as shown in Fig. 8 from converted, 22-bit digital PPG waveforms. With PPTs in hand, DBPs and SBPs can be then calculated based on Eqs. (4) and (9). The obtained DBPs and SBPs are shown in correlation plots as opposed to the measurement by HEM-7310 in Fig. 15(a, b), and Bland–Altman plots in Fig. 16(a, b), along with their counterparts by two other commercial modules. It is seen from Fig. 15(a,b) that the developed sensor renders correlations of 0.95 for SBPs while 0.98 for

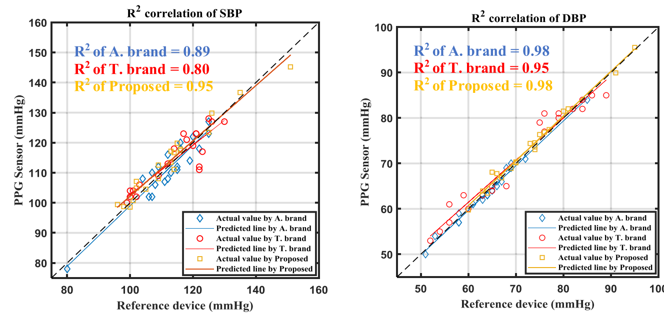

(a) (b)

Fig. 15. Correlation plots of (a) SBPs and (b) DBPs.

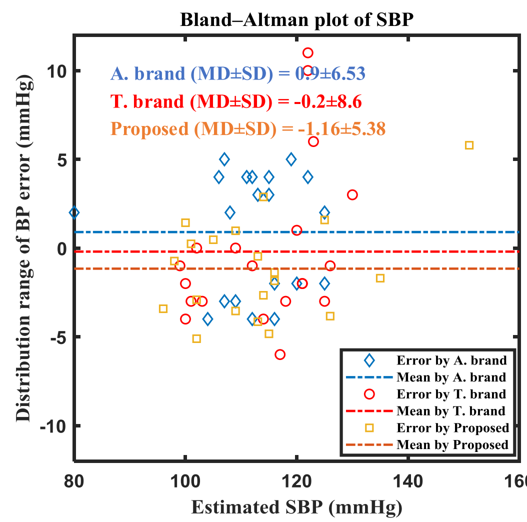

(a)

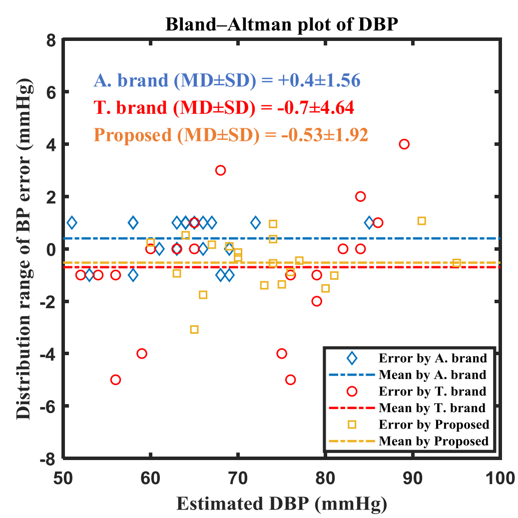

(b)

Fig. 16. The associated Bland–Altman plots of (a) SBP, (b) DBP.

DBPs, considerably high correlations. On the other hand, these obtained correlations are better than or equal to those by the two other commercial modules. It can be also seen from Fig. 16(a,b) that the mean difference (MD) and standard deviation (SD) associated with the measurement errors are -1.16 ± 5.38 mmHg (MD±SD) and -0.53 ± 1.92 mmHg, respectively, for SBP and

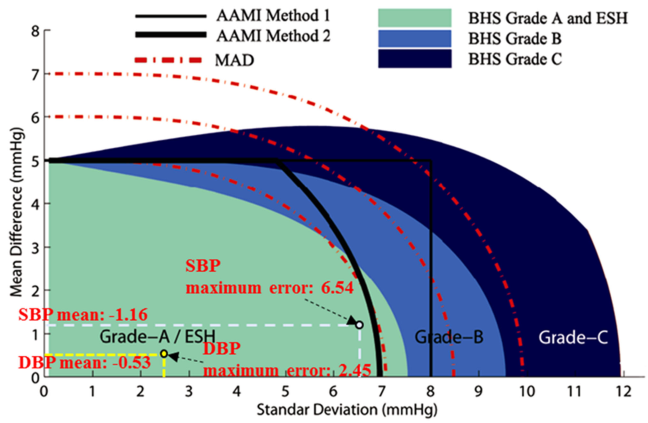

Fig. 17. Summary of varied standards of accuracy by [40] for a wearable BP sensing devices.

DBP. The accuracy obtained by the proposed PPG module in terms of the confidence interval corresponding to 1.96 times of standard deviation are smaller than all the counterparts by the two other commercial modules, expect for that for DBP by Brand A. Since the performance by the proposed module is much better than Brand A's Model 03 for estimating SBP, i.e., 5.38 versus 6.53, as opposed to a slightly larger confidence internal, 1.92 versus 1.56, in DBP, the proposed module can still be considered better than Brand A. Finally, according to the standards set up by the Association for the Advancement of Medical Instrumentation (AAMI) [38] and the British Hypertension Society (BHS) [39] documented by [40], the proposed PPG sensor achieves an accuracy in the categories of method 2 (the best accuracy) by AAMI while Grade A (the highest grade) by BHS as given in Fig. 17, resulting in relatively high accuracy among varied cuffless BP sensors. However, it should be noted at this point that despite the relatively high accuracy obtained herein, this is in part due to that fact that all study subjects are relatively healthy, as seen in Table III. The subject group can be expanded in the future for further exploration on accuracy.

VI. Conclusion

A new LEDs/PD module is designed and fabricated for measuring quality PPG waveforms to achieve high-accuracy biosensing. Effort was dedicated to establish a thorough model of optical simulation for finding the optimal distances between LEDs and PD in the module for different wavelengths. In results, an AC/DC ratio of 8.02% is achieved by the proposed PPG module as opposed to 6.74 and 6.90% by two other commercial modules. This optimized module was further installed in a handheld blood pressure (BP) monitor device developed by this lab to demonstrate its effectiveness of estimating BPs. Measurements by this device show that with the developed LEDs/PD module, the estimation error can be controlled well with the MD and SD as -1.16 ± 5.38 and -0.53 ± 1.92 mmHg, respectively, for SBP and DBP. The result conforms to Grade A (the highest grade) by BHS and the categories of method 2 (the best accuracy) by AAMI.

References

[1] L. Feng, L. M. Po, X. Xu, Y. Li, and R Ma, "Motion-resistant remote imaging photoplethysmography based on the optical properties of skin," *IEEE Trans. Circuits Syst.*, vol. 25, no. 5, pp. 879–891, May 2015.

[2] K. Matsumura, T. Yamakoshi, P. Rolfe, and K. I. Yamakoshi, "Advanced volume-compensation method for indirect finger arterial pressure determination: Comparison with brachial sphygmomanometry," *IEEE Trans. Biomed. Eng.*, vol. 64, no. 5, pp. 1131–1137, May 2017.

[3] K. N. Karmali and D. M. Lloyd-Jones, "Global risk assessment to guide blood pressure management in cardiovascular disease prevention," *Hypertension*, vol. 69, no. 3, pp. 2–9, 2017.

[4] D. Ettehad *et al.*, "Blood pressure lowering for prevention of cardiovascular disease and death: A systematic review and meta-analysis," *Lancet*, vol. 387, no. 10022, pp. 957–967, 2016.

[5] P. M. Nabeel, S. Karthik, J. Joseph, and M. Sivaprakasam, "Arterial blood pressure estimation from local pulse wave velocity using dual-element photoplethysmograph probe," *IEEE Trans. Instrum. Meas.*, vol. 67, no. 6, pp. 1399–1408, Jun. 2018.

[6] X. R. Ding, Y. T. Zhang, J. Liu, W. X. Dai, and H. K. Tsang, "Continuous cuffless blood pressure estimation using pulse transit time and photoplethysmogram intensity ratio," *IEEE Trans. Biomed. Eng.*, vol. 63, no. 5, pp. 964–972, May 2016.

[7] E. Kaniusas *et al.*, "Method for continuous nondisturbing monitoring of blood pressure by magnetoelastic skin curvature sensor and ECG," *IEEE Sensors J.*, vol. 6, no. 3, pp. 819–828, Jun. 2006.

[8] T.-Y. Tu, P. C.-P. Chao, and Y.-P. Lee, "A new non-invasive cuff-less blood pressure sensor," in *Proc. IEEE Sensors*, Baltimore, MD, USA, Nov. 2013, pp. 1–4.

[9] T.-Y. Tu, Y. H. Kao, P. C. Chao, and Y. P. Lee, "Optimizing a new blood pressure sensor for maximum performance based on finite element model," in *Proc. Conf. IEEE Sensors*, Valencia, Spain, 2014, pp. 1873–1876.

[10] Y.-H. Kao, T. Y. Tu, Paul C. P. Chao, Y. P. Lee, and C. L. Wey, "Optimizing a new cuffless blood pressure sensor via a solid-fluid-electric finite element modeling with consideration of varied Mis-positionings," *J. Microsyst. Technol.*, vol. 22, pp. 1437–1447, Jun. 2016.

[11] Y.-H. Kao, P. C. P. Chao, Y. Hung, and C. L. Wey, "A new reflective PPG LED-PD sensor module for cuffless blood pressure measurement at wrist artery," in *Proc. IEEE SENSORS Conf.*, 2017, pp. 1–3.

[12] V. O. Rybynok and P. A. Kyriacou, "Beer-lambert law along non-linear mean light pathways for the rational analysis of photoplethysmography," *J. Phys.: Conf. Series*, vol. 238, no. 1, 2010, Art. no. 012061.

[13] C. Mansouri and N. H. Kashou, "New window on optical brain imaging; medical development, simulations and applications," in *Selected Topics on Optical Fiber Technology*. Rijeka, Croatia: InTech, 2012, pp. 271–289.

[14] R. Mukherjee, S. Dubey, B. Gupta, and T. Chakravarty, "Bio-optical modeling of human skin to eliminate the skin structure variability in blood pressure measurement," in *Proc. Conf. IEEE Advances Elect., Electron., Inf., Commun. Bio-Informat.*, 2016, pp. 450–454.

[15] M. J. C. van Gemert, S. L. Jacques, H. J. C. M. Sterenborg, and W. M. Star, "Skin optics," *IEEE Trans. Biomed. Eng.*, vol. 36, no. 12, pp. 1146–1154, Dec. 1989.

[16] A. Reisner, P. A. Shaltis, D. McCombie, and H. H. Asada, "Utility of the photoplethysmogram in circulatory monitoring," *Anesthesiology*, vol. 108, no. 5, pp. 950–958, 2008.

[17] A. Liopo, R. Su, D. A. Tsyboulski, and A. A. Oraevsky, "Optical clearing of skin enhanced with hyaluronic acid for increased contrast of optoacoustic imaging," *J. Biomed. Opt.*, vol. 21, no. 8, 2016, Art. no. 081208.

[18] J. Allen, "Photoplethysmography and its application in clinical physiological measurement," *Physiol. Meas.*, vol. 28, no. 3, pp. 1–39, Mar. 2007.

[19] X. B. D. Pham *et al.*, "Racial and gender differences in arterial anatomy of the arm," *Amer. Surgeon*, vol. 82, no. 10, 973–976, 2016.

[20] P. Adhikari, W. Eklund, E. A. Sherer, and D. P. O'Neal, "Assessment of multi-wavelength pulse photometry for non-invasive dose estimation of circulating drugs and nanoparticles," *Proc. SPIE*, vol. 9715, 2016, Art. no. 97150O.

[21] V. V. Tuchin, "Light scattering study of tissues," *Physics-Uspekhi*, vol. 40, pp. 495–515, 1997.

[22] R. Splinter and B. A. Hooper, *An Introduction to Biomedical Optics (Optics and Optoelectronics)*. New York, NY, USA: Taylor & Francis, 2006.

[23] A. A. Kamshilin and N. B. Margaryants, "Origin of photoplethysmographic waveform at green light, " *Phys. Procedia*, vol. 86, pp. 72–80, 2017.

[24] J. Kim *et al.*, "Miniaturized battery-free wireless systems for wearable pulse oximetry," *Adv. Functional Mater.*, vol. 27, no. 1, 2017.

[25] R. Sato, M. Kato, K. Kurihara, and E. Okada, "Wavelength dependence of partial optical path length in the vascular plexus of reflected light of the skin," in *Proc. Clinical Translational Biophotonics*, 2016, Paper JM3A-31.

[26] M. Huotari, J. Röning, and K. Määttä, "Infrared and red PPG signals analysis of the healthy subjects and clinical patients," in *Proc. Biennial Baltic Electron. Conf.*, 2016, pp. 111–114.

[27] A. Alzahrani *et al.*, "A multi-channel opto-electronic sensor to accurately monitor heart rate against motion artefact during exercise," *Sensors*, vol. 15, pp. 25681–25702, 2015.

[28] Y. H. Kao, P. C. P. Chao, and C. L. Wey, "Towards maximizing the sensing accuracy of an cuffless, optical blood pressure sensor using a high-order front-end filter," *Microsyst. Technol.*, pp. 1–10, 2018.

[29] J. C. Bramwell and A. V. Hill, "The velocity of the pulse wave in man," *Proc. Roy. Soc. London Biol. Character*, vol. 93, no. 652, pp. 298–306, 1922.

[30] F. N. Van de Voss and N. Stergiopulos, "Pulse wave propagation in the arterial tree," *Annu. Rev. Fluid Mechanics*, vol. 43, pp. 467–499, 2011.

[31] D. N. Ku, "Blood flow in arteries," *Annu. Rev. Fluid Mechanics*, vol. 29, no. 1, pp. 399–434, 1997.

[32] M. F. O'rourke, "Vascular impedance in studies of arterial and cardiac function," *Physiol. Rev.*, vol. 62, no. 2, pp. 570–623, 1982.

[33] H. Shin and S. D. Min, "Feasibility study for the non-invasive blood pressure estimation based on PPG morphology: Normotensive subject study," *Biomed. Eng. Online*, vol. 16, no. 1, pp. 1–14, 2017.

[34] D. McDuf, S. Gontarek, and R. W. Picard, "Remote detection of photoplethysmographic systolic and diastolic peaks using a digital camera," *IEEE Trans. Biomed. Eng.*, vol. 61, no. 12, pp. 2948–2954, Dec. 2014.

[35] A. I. Moens, *Die Pulscurve*. Leiden, The Netherlands: E. J. Brill, 1878.

[36] D. J. Korteweg, "Ueber die Fortpflanzungsgeschwindigkeit des Schalles in elastischen Röhren," *Annalen der Physik*, vol. 241, no. 12, pp. 525–542, 1878.

[37] A. J. Bank *et al.*, "Direct effects of smooth muscle relaxation and contraction on in vivo human brachial artery elastic properties," *Circulation Res.*, vol. 77, pp. 1008–1016, 1995.

[38] Association for the Advancement of Medical Instrumentation, "Noninvasive sphygmomanometers—Part 2: Clinical investigation of automated measurement type," ANSI/AAMI/ISO 81060-2:2013, Arlington, VA, USA, 2016.

[39] E. O'brien *et al.*, "The British Hypertension Society protocol for the evaluation of automated and semi-automated blood pressure measuring devices with special reference to ambulatory systems," *J. Hypertension*, vol. 8, pp. 607–619, 1990.

[40] IEEE Standards Association, *IEEE Standard for Wearable Cuffless Blood Pressure Measuring Devices*, IEEE Standard, 2014.

Yung-Hua Kao received the M.S. degree from Chung Yuan Christian University, Taoyuan, Taiwan. He is currently working toward the Ph.D. degree at the Electrical and Computer Engineering Department, National Chiao Tung University, Hsinchu, Taiwan. He has an experience of part-time Researcher for analysis of frontal EEG asymmetry for depressed patients in National Taiwan University Hospital, 2012–2013. He has also work experiences of part-time Engineer, to develop the sensor for blood pressure, Maisense Inc., 2013–2014. His research interests focus on the optical-sensor development, analog circuit design, algorithm development, and system integration. He was the recipient of the 2014/2016 Best Paper Award from the 25/27th Annual ASME Conference on Information Storage and Processing Systems, Santa Clara, CA, USA, and the 13th National Innovation Award from 2016 Institute for Biotechnology and Medicine Industry. He was also the recipient of the Future Technology Award (Taiwan Oscar Invention Award) from Ministry of Science and Technology, Taiwan, 2017.

Paul C.-P. Chao received the Ph.D. degree from Michigan State University, East Lansing, MI, USA. After graduation, he was with the CAE Department, Chrysler Corporation, Auburn Hill, MI, USA, for two years. He is currently the University Distinguished Professor with Electrical Engineering Department, National Chiao Tung University (NCTU), Hsinchu, Taiwan, and an IEEE Distinguished Lecturer. His research interests focus on circuit designs for sensors and actuators; micro-mechatronics and control technology. He was the Secretary General of IEEE Taipei Section, 2009–2010, and the Founding Chair of local chapter for the IEEE Sensor Council. He is an ASME Fellow. For editorial services, he is the Topical Editor for the IEEE SENSORS JOURNAL and the IEEE INTERNET OF THINGS JOURNAL, and also the Associate Editors for the *ASME Journal of Vibration and Acoustics* and the *Journal of Circuit, System and Computer*. He was the General Chair of the 2016 ASME ISPS and IoT conference, Santa Clara, CA, USA. He was the University Associate VPs of NCTU for academic affairs and for research and development. He was the recipient of the 1999 Arch T. Colwell Merit Best Paper Award from Society of Automotive Engineering, Detroit, MI, USA; the 2004 Long-Wen Tsai Best Paper Award from National Society of Machine Theory and Mechanism, Taiwan; and the 2005 Best Paper Award from National Society of Engineers, Taiwan. He was the recipient of the University Distinguished Professor in 2014, and the prestigious Outstanding Research Award from National Association of Automatic Control of Taiwan in 2015 and National Society of Engineers of Taiwan in 2017. He was also the recipient of two IEEE awards for this service: The IEEE Large Section Award from IEEE Head Quarter for the outstanding service as the Secretary for 2009–2010, and the IEEE MGA Award from IEEE Region 10 for outstanding service as the Secretary for IEEE Taipei Section, 2009–2010.

Chin-Long Wey (M'83–SM'97–F'11–LF'17) received the Ph.D. degree in electrical engineering from Texas Tech University, Lubbock, TX, USA, in 1983. He is currently the Chair Professor of the Electrical and Computer Engineering Department, National Chiao Tung University, Hsinchu, Taiwan. He was the Director General of the National Chip Implementation Center, Hsinchu, Taiwan, in 2007–2010, and the Dean of the College of Electrical Engineering and Computer Science, National Central University (NCU), in 2003–2006. He came to NCU from Michigan State University where he was a Full Professor with Electrical and Computer Engineering Department from 1983 to 2003 for 20 years. In 2001, he started up a Fab-less design house, JMicron Technology Corp., Hsinchu, Taiwan, that develops and markets high-speed serial link products. His research interests include design, testing, and fault diagnosis of high-speed analog/mixed-signal VLSI circuits and systems; and power management systems. He is a Fellow of the US National Academy of Inventor.